Journal of Geophysical Research: Atmospheres

RESEARCH ARTICLE
10.1002/2017JD028243

How Accurately Can the Air Temperature Lapse Rate Over the Tibetan Plateau Be Estimated From MODIS LSTs?

Hongbo Zhang[1], Fan Zhang[1,2,3], Guoqing Zhang[1,2], Tao Che[2,4], and Wei Yan[1]

[1]Key Laboratory of Tibetan Environment Changes and Land Surface Processes, Institute of Tibetan Plateau Research, Chinese Academy of Sciences, Beijing, China, [2]CAS Center for Excellence in Tibetan Plateau Earth Sciences, Beijing, China, [3]Institute of Tibetan Plateau Research, University of Chinese Academy of Sciences, Beijing, China, [4]Cold and Arid Regions Environmental and Engineering Research Institute, Chinese Academy of Sciences, Beijing, China

Abstract The air temperature lapse rate (TLR) is a key parameter for interpolating air temperature data in high mountainous regions such as the Tibetan Plateau (TP). The Moderate Resolution Imaging Spectroradiometer (MODIS) land surface temperature (LST) has been frequently used for estimating air temperature during the past decade, but its performance in estimating the TLR in the TP has seldom been investigated. This study employed two methods in estimating the TLR based on MODIS LSTs compared with the "observed" TLR derived from 86 stations across the TP. The two methods include a method for directly computing the lapse rate from MODIS LST (DFM) and a second method for calculating the lapse rate of estimated air temperatures based on air temperature estimation from MODIS LST (TEM). The results show that the MODIS LST-estimated TLR for daily mean air temperature (*T*mean) using both DFM and TEM is more accurate than that for daily minimum and maximum air temperatures. When using MODIS nighttime LSTs, both DFM and TEM show acceptable accuracies for estimating the TLR of *T*mean with averaged root-mean-square deviations of 0.21 and 0.19 °C/100 m, respectively. The spatial and seasonal patterns of MODIS LST-estimated TLRs of *T*mean from both DFM and TEM are found to be highly consistent with the observed TLRs. This study can help alleviate the data-sparse problem in downscaling air temperature or hydrological modeling studies in ungauged areas, especially for the western TP where station data are extremely scarce.

Key Points:
- Both DFM and TEM show acceptable accuracies for estimating the TLR of *T*mean using MODIS nighttime LSTs with mean RMSDs of ~0.2 °C/100 m
- The MODIS LST-estimated TLR for *T*mean is more accurate than that of *T*min and *T*max
- The monthly TLR of *T*mean can be simulated by directly computing the lapse rates of the MODIS nighttime LSTs

Supporting Information:
- Supporting Information S1

Correspondence to:
F. Zhang,
zhangfan@itpcas.ac.cn

Citation:
Zhang, H., Zhang, F., Zhang, G., Che, T., & Yan, W. (2018). How accurately can the air temperature lapse rate over the Tibetan Plateau be estimated from MODIS LSTs? *Journal of Geophysical Research: Atmospheres*, *123*. https://doi.org/10.1002/2017JD028243

Received 24 DEC 2017
Accepted 23 MAR 2018
Accepted article online 30 MAR 2018

1. Introduction

Air temperature is an important variable for numerous studies related to ecology (Hänninen et al., 2013; Kollas et al., 2014), hydrology (L. Wang et al., 2016), and climate change (Cai et al., 2016). Air temperature is a very important factor for many hydrological (Minder et al., 2010) and ecological processes (Ma et al., 2017; Walther et al., 2002; Wu et al., 2012), particularly for those in cold regions (Kang et al., 2010). For hydrological modeling in mountainous or glacierized basins, air temperature is the key input for snow or glacier melt simulations (F. Zhang et al., 2015). Air temperature data are also the basis of global and regional warming analysis (X. Liu & Chen, 2000; Pepin et al., 2015; W. Xu & Liu, 2007). However, accurate air temperature data are difficult to obtain due to the sparse observations in high mountainous areas, such as the Tibetan Plateau (TP). The TP has an average altitude of ~4,000 m, and most of meteorological stations are located at low elevations (<4,000 m) and in the eastern plateau. The problem of sparse air temperature data is more severe in the western TP.

As a strong negative relation of air temperature with elevation, the air temperature lapse rate (TLR) is commonly used for interpolating air temperature in mountainous areas (Dobrowski et al., 2009; Dodson & Marks, 1997; Petersen et al., 2013). Quantifying the spatial distribution of air temperature, which is commonly described by TLR, is the basis for accurately simulating a number of hydrological and ecological processes, including evapotranspiration (Ma et al., 2015), distinguishing snow and rainfall (Ding et al., 2014), snow and glacier melting (T. G. Gao et al., 2015; F. Zhang et al., 2015), and tree species' distribution (Kollas et al., 2014) in high elevation areas. In addition, TLR is frequently used for downscaling large-scale air temperature data sets in regional climate model (Lilleøren et al., 2013; Nilsson, 2009) and for creating grid temperature input in hydrological models (Luo et al., 2013; Sun et al., 2013; L. Zhang et al., 2013) to investigate the regional response to climate change. The TLR is usually estimated through linear regression based on air temperature observations at neighboring stations (Immerzeel et al., 2014). A constant value of 0.55–0.65 °C/100 m has

been widely used for the TLR (Arnold et al., 2006), but it could vary in both space and time (X. Li et al., 2013). Based on station observations of air temperature, a number of studies have analyzed the spatial and seasonal variation of TLR in the TP (Guo et al., 2016; Kattel et al., 2013, 2015, 2017; X. Li et al., 2013; Y. Li et al., 2015; Yang et al., 2011). The TP is found to have a steeper TLR and a distinct seasonal pattern of TLR than the other parts of China (X. Li et al., 2013; Y. Li et al., 2015). Generally, a strong seasonal pattern of TLR is found in the TP with a shallower TLR in summer and a steeper one in winter (Kattel et al., 2015; X. Li et al., 2013; Y. Li et al., 2015). A bimodal seasonal pattern is also found in some areas of the TP such as the Himalayan regions with two maxima in premonsoon and postmonsoon seasons (Kattel et al., 2013, 2017). The spatial variation of TLR over the TP is also significant according to Guo et al. (2016) and Y. Li et al. (2015), and distinct seasonal patterns of TLR are observed between the southern and northern slopes of the Himalayas (Kattel et al., 2015). These studies indicate that the TLR of the TP may only be locally accurate due to the effects of microclimates (e.g., humidity) and terrain conditions (Kattel et al., 2013, 2015; Minder et al., 2010). The accurate estimation of the TLR largely relies on sufficiently dense and representative observations. However, the sparse distribution of stations in the TP, especially in high-altitude regions, may lead to a large bias (Immerzeel et al., 2014).

Remotely sensed land surface temperature (LST) can provide comprehensive temperature observations compared with the limited ground stations (Z.-L. Li et al., 2013). Remotely sensed LSTs, especially the Moderate Resolution Imaging Spectroradiometer (MODIS) LST data, are generally used for air temperature estimation in mountainous areas around the world based on the strong correlation between the air temperature and the LST (Benali et al., 2012; Cristobal et al., 2008; Kilibarda et al., 2014; Lin et al., 2016; C. Liu et al., 2013; Meyer et al., 2016; Park, 2011; Peon et al., 2014; Pepin et al., 2016; Qu et al., 2011; W. Zhang et al., 2011) including the TP (Fu et al., 2011; Y. H. Yao & Zhang, 2013; H. Zhang, Zhang, Ye, et al., 2016; H. Zhang et al., 2018; Zhu et al., 2013). Various statistical methods including simple linear regression (Fu et al., 2011; W. Zhang et al., 2011) and complex models such as the M5 model tree (Emamifar et al., 2013) and the random forest predicting model (Y. Xu et al., 2014) have been developed for air temperature estimation. In addition to MODIS LSTs, some auxiliary variables including elevation, latitude, longitude, and Julian day are also included in models for more accurate estimations (Benali et al., 2012; Y. Xu et al., 2014; H. Zhang, Zhang, Ye, et al., 2016). However, the air temperature data produced by these methods are seldom used in the estimation of the TLR.

Actually, the MODIS LST data alone have the potential to directly reflect the spatial variation of air temperature (Shamir & Georgakakos, 2014). For example, L. Wang et al. (2016) found that the modeling results were improved using the lapse rate of the MODIS nighttime LST as the TLR in snowmelt modeling for the upper Yellow River basin. Using subhourly *T*air observations in Nevada, Mutiibwa et al. (2015) found the mean difference of the instantaneous *T*air TLR and the MODIS LST TLR for nighttime is much smaller than that for daytime. Similarly, Oyler et al. (2016) indicated that the spatial variability of MODIS daytime LST is much larger than that of *T*max, while the spatial patterns of MODIS nighttime LST and *T*min are very similar. Thus, there are at least two methods that can be used to estimate the TLR, including one method computed directly from MODIS LSTs (referred to as "DFM") and a method based on air temperature estimation from MODIS LSTs in combination with auxiliary variables (referred to as "TEM").

Generally, three types of daily air temperatures are interpolated using the TLR, including the daily mean (*T*mean), minimum (*T*min, and maximum (*T*max) air temperatures. The TLR of *T*mean is the most commonly used. The *T*min and *T*max are also important for a number of ecological studies (Hänninen et al., 2013; Kollas et al., 2014; Tonini et al., 2016). MODIS instruments are onboard two satellites (Terra and Aqua) with two daily observations (daytime and nighttime) each. The MODIS nighttime LST has typically been used for the estimation of *T*min and is also recommended for the estimation of *T*mean (W. Zhang et al., 2011; H. Zhang, Zhang, Ye, et al., 2016). The MODIS daytime LST has been commonly used for the estimation of *T*max (Y. Xu et al., 2014; Zhu et al., 2013); however, the MODIS nighttime LST was found to present even better accuracy for the estimation of *T*max (W. Zhang et al., 2011). The estimation accuracies for *T*mean and *T*min are better than that of *T*max (Benali et al., 2012; H. Zhang, Zhang, Zhang, et al., 2016). However, errors induced by undetected clouds and the mixed-pixel effects may affect the *T*air estimation accuracies (H. Zhang, Zhang, Zhang, et al., 2016) and thus affect the TLR estimation using the TEM method.

Thus, whether the methods of DFM and TEM which both use MODIS LST data are feasible for estimating the TLR, and how the accuracies produced by the two methods are affected by the three types of *T*air and the four MODIS pass times all remain unknown. Making clear these questions is very important and urgent for

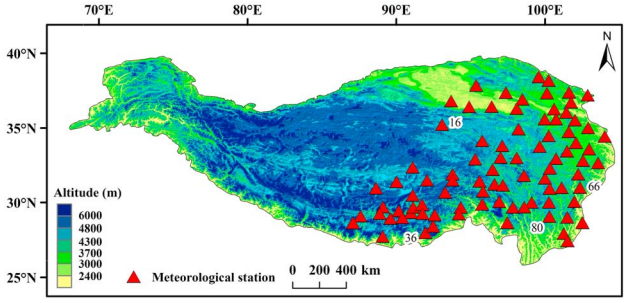

Figure 1. Study area and locations of 86 China Meteorological Administration stations. The altitude data were derived from the Shuttle Radar Topography Mission at a spatial resolution of 90 m.

obtaining more spatially representative TLRs to get more accurate spatial distribution of air temperature of the TP where meteorological stations are extremely sparse. In fact, more accurate estimations of the TLR are also important for many other regions with sparse stations, such as the Cascade Mountains in North America (Minder et al., 2010) and the Prince of Wales Icefield in Canada (Marshall et al., 2007). To our knowledge, there has been no study that focuses on estimating the TLR from MODIS LST data by using the DFM or TEM method considering different types of *T*air (*T*mean, *T*min, and *T*max) and different MODIS pass times.

In this study, three main questions are raised: (1) How accurately can the air TLR be estimated from MODIS LSTs? (2) Which of the two methods, DFM or TEM, is better for estimating the TLR? and (3) Among the TLRs for *T*mean, *T*min, and *T*max, which TLR is best estimated from MODIS LSTs? To answer these questions, we employed both the DFM and TEM methods to estimate the monthly TLRs from MODIS LST data; The accuracies of TLR estimations for *T*mean, *T*min, and *T*max were then calculated and compared for each method, in comparison to the observed TLRs derived based on 86 stations located across the TP.

2. Data Used

2.1. Meteorological Station Data

The TP covers a large area of about 3×10^6 km^2 (G. Zhang et al., 2013). The elevation ranges from ~2,000 to ~8,800 m (Figure 1). Due to the high elevation and low temperature, snow and glaciers are widespread resulting in that the TP is among the most sensitive areas to climate warming (T. Yao et al., 2012). This study focuses on the southern and eastern TP covering an area of ~1.4×10^6 km^2, as most of China Meteorological Administration (CMA) stations are located there and a reliable calculation of TLR requires sufficient neighboring stations. The latitude and longitude ranges of the stations are 27.43–38.42°N and 87.08–104.02°E, respectively. The altitudes of all stations range from 1,660 to 4,800 m. Daily observations of *T*max, *T*min, *T*mean, precipitation, sunshine duration, vapor pressure, wind speed, and relative humidity of 8 years (2003–2010) from 86 available CMA stations were used. Very few observation data during the study period are missing with the proportion of less than 0.02%. All the air temperature observations are measured at 2 m above ground. Elevation, altitude, and latitude/longitude information of the 86 stations were also obtained from CMA.

2.2. MODIS LST

Daily LST data at 1-km resolution from the data sets of "MODIS/Terra Land Surface Temperature and Emissivity Daily L3 Global 1 km Grid SIN V006" (MOD11A1) and "MODIS/Aqua Land Surface Temperature and Emissivity Daily L3 Global 1 km Grid SIN V006" (MYD11A1) were used. They are the latest MODIS LST versions that are claimed to improve the accuracy and stability of the LST data (Wan, 2014). Both MOD11A1 and MYD11A1 provide two data per day including a daytime and a nighttime observation. They are Terra night (LST_{TN}), Terra day (LST_{TD}), Aqua night (LST_{AN}), and Aqua day (LST_{AD}), which are observed at 22:30, 10:30, 1:30, and 13:30 local time, respectively. Terra day and night LSTs are considered to be better proxies for estimating *T*max and *T*min, respectively (Zhu et al., 2013). Besides the LST data, each data grid is accompanied with a flag indicating the data quality. The flag values of 0–3 represent the average errors of <1, 1–2, 2–3, and >3 K, respectively. In this study, all the data with flag value of 3 were removed to maintain quality of the LST data being used. It should be noted that only the LST values of the MODIS pixels where the corresponding CMA stations (totally 86) located were used for a fair comparison. In addition, only days with four MODIS LST observations without cloud coverage were used to ensure a reliable comparison among them. The geolocation error of MODIS data is archived to be ~50 m at nadir (Wolfe et al., 2002). This error is considered small, and the LST data of the MODIS pixels (1 km) where meteorological stations are located within are often directly used for temperature comparison (Hachem et al., 2012) or for air temperature estimation studies (Benali et al., 2012; Emamifar et al., 2013; H. Zhang, Zhang, Ye, et al., 2016). In this study, we followed the same way. It should be noted that Terra and Aqua LST data are available from 24 February 2000 to 4 July 2002, respectively. Thus, the study period starts from 2003 when both Terra and Aqua have full-year observations

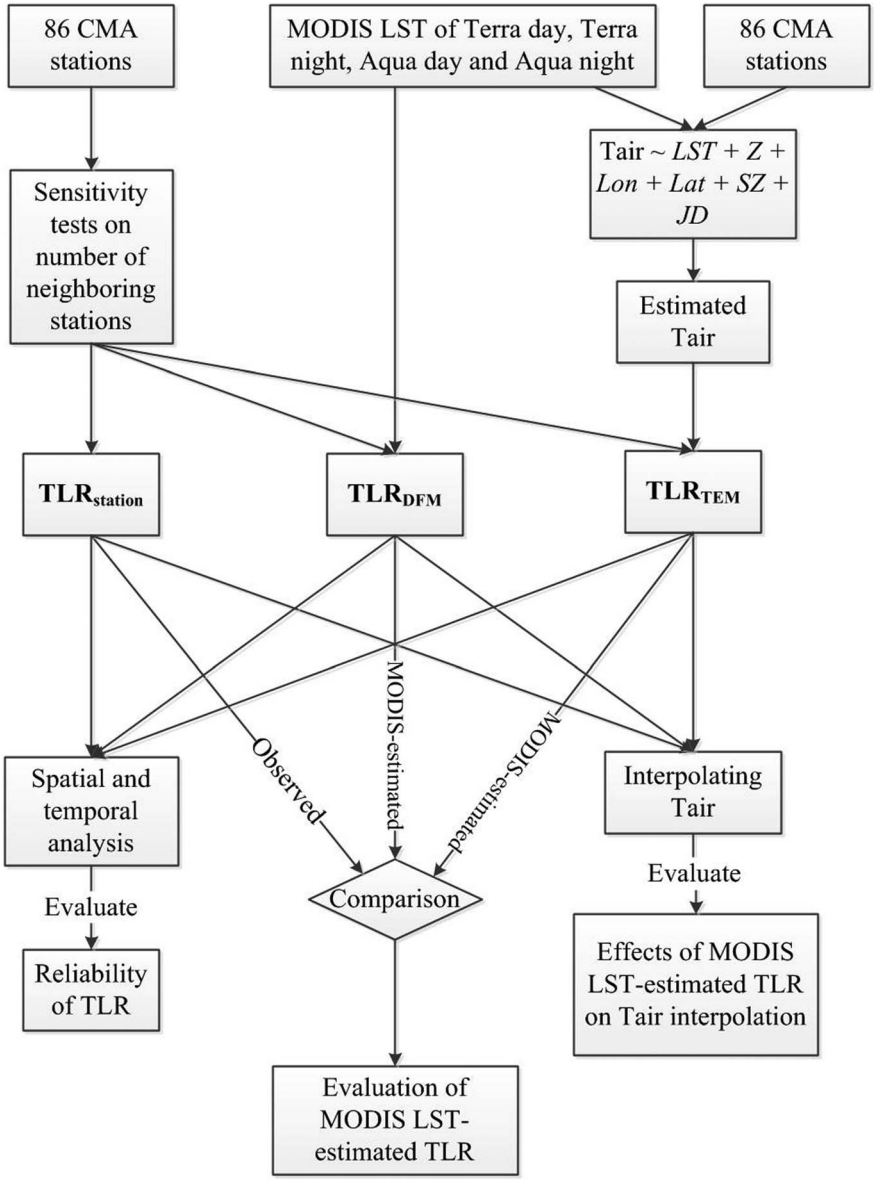

Figure 2. The flow chart describing how the Moderate Resolution Imaging Spectroradiometer (MODIS) land surface temperature (LST)-estimated temperature lapse rate (TLR), including TLR_{DFM} and TLR_{TEM} was produced, evaluated and analyzed. "Z" is elevation, "Lat" is latitude, "Lon" is longitude, "SZ" is solar zenith, and "JD" is Julian day. CMA = China Meteorological Administration.

and last to 2010 to when 8-year LST data can be acquired and are expected to be sufficient for analysis. The study period is also consistent with the meteorological station data we obtained.

3. Methods

3.1. Estimating TLR

Three types of TLR are defined in this study, that is, (1) the estimated TLR based on the *T*air data from neighboring CMA stations, referred to as "$TLR_{station}$," which is designated as the observed (or true) TLR; (2) the MODIS LST-estimated TLR using the DFM method, referred to as "TLR_{DFM}"; and (3) the MODIS LST-estimated TLR using the TEM method, referred to as "TLR_{TEM}." Figure 2 shows the procedure for estimating, evaluating, and analyzing the three types of TLR.

3.1.1. Estimation of $TLR_{station}$

$TLR_{station}$ is calculated through a linear regression between air temperature and the elevations of selected neighboring stations using equation (1):

$$T\text{air} = a \times Z + b \tag{1}$$

where *T*air is air temperature, *Z* is elevation, *a* and *b* are both regression coefficients, and the value of *a* is taken as the $TLR_{station}$. The longitude or latitude is also considered for calculating the TLR in some studies (X. Li et al., 2013; Rolland, 2003). Due to the possibly serious multicollinearity problem found in this study as indicated in the supporting information (Text S1; Craney & Surles, 2002), only elevation is considered in equation (1). The neighboring stations for computing TLR are usually determined by collecting available stations within a specific area such as a basin (F. Zhang et al., 2015) and a latitude-longitude divided region (X. Li et al., 2013) or using a fixed number (e.g., 20; Y. Li et al., 2015). Considering that the TLR is locally accurate and that the TLR is feasible only when the air temperature has a strong correlation with elevation, the neighboring stations in this study are selected using a sensitivity test as follows: for each CMA station, the nearest neighboring CMA stations were added sequentially. Once a new station was added, the TLR and the correlation coefficient (*R*) and its significance level were computed. This process continued until a strong negative correlation was indicated at the 0.05 significance level, and the corresponding station number was selected as the number of neighboring stations. This process was repeated for all the 86 CMA stations. This method has been successfully applied to determine the reasonable number of neighboring stations for four glacier sites of the TP (H. Zhang et al., 2018). It should be noted that the daily mean air temperature data during 2003–2010 were used in this process. Lastly, local daily $TLR_{station}$ values for the three types of daily *T*air, including TLR_{Tmax}, TLR_{Tmean}, and TLR_{Tmin} were computed for every CMA station.

Spatial and temporal analyses were then conducted to evaluate how reasonable the $TLR_{station}$ values were. Monthly variations of $TLR_{station}$ were investigated first. It should be noted that 12 multiyear average, monthly $TLR_{station}$ values were derived from the corresponding daily $TLR_{station}$ values for the study period (2003–2010). The multiyear average, monthly TLR was used in a modeling study in southern TP and proved to be efficient (F. Zhang et al., 2015). The spatial distribution characteristics of $TLR_{station}$s were analyzed as follows: For each station, an aggregate average $TLR_{station}$ during 2003–2010 was calculated. A correlation analysis was then conducted by examining the relationship between the $TLR_{station}$s and 10 terrain/meteorological factors using the Pearson correlation coefficient as measurement. The 10 factors are (1) the maximum distance to the farthest neighboring station (referred to as "max distance"), (2) altitude, (3) longitude, (4) latitude, (5) precipitation, (6) sunshine duration, (7) air temperature, (8) vapor pressure, (9) wind speed, and (10) relative humidity.

3.1.2. Estimation of TLR_{DFM}

Because there are four terms of MODIS LST observations per day including LST_{TN}, LST_{TD}, LST_{AN}, and LST_{AD}, the corresponding four sets of daily TLR_{DFM} values can be calculated using equations (2)–(5):

$$LST_{TN} = a_1 \times Z + b_1 \tag{2}$$

$$LST_{TD} = a_2 \times Z + b_2 \tag{3}$$

$$LST_{AN} = a_3 \times Z + b_3 \tag{4}$$

$$LST_{AD} = a_4 \times Z + b_4 \tag{5}$$

where a_1, a_2, … b_1, … and b_4 are regression coefficients and a_1, a_2, a_3, and a_4 are the TLR_{DFM} values for the four different MODIS LST terms, respectively. The neighboring stations/grids used were the same as those used for $TLR_{station}$. It should be noted that for each MODIS LST term, the TLR_{DFM} is directly compared with the TLR_{Tmax}, TLR_{Tmean}, and TLR_{Tmin} values from $TLR_{station}$ to evaluate its accuracy for estimations of the three types of TLR. Similar to $TLR_{station}$, the 12 multiyear average, monthly TLR_{DFM} values were derived from the corresponding daily TLR_{DFM} values for the study period (2003–2010). For example, when calculating the monthly TLR_{DFM} for station no. 6 with its neighboring stations of nos. 4, 5, 10, 11, 15, and 18, the LST data from the

totally seven pixels were first used for calculating daily TLR_{DFM}. All the available daily TLR_{DFM} were then aggregated to calculate the multiyear average, monthly TLR_{DFM} values.

3.1.3. Estimation of TLR_{TEM}

Twelve sets of *T*air (four sets for each of *T*max, *T*min, and *T*mean) were initially estimated based on four MODIS LST terms using simple multiple linear regression equations (6)–(9):

$$T_{air} = a_1 \times LST_{TN} + b_1 \times Z + c_1 \times SZ + d_1 \times Lon + e_1 \times Lat + f_1 \times JD + g_1 \quad (6)$$

$$T_{air} = a_2 \times LST_{TD} + b_2 \times Z + c_2 \times SZ + d_2 \times Lon + e_2 \times Lat + f_2 \times JD + g_2 \quad (7)$$

$$T_{air} = a_3 \times LST_{AN} + b_3 \times Z + c_3 \times SZ + d_3 \times Lon + e_3 \times Lat + f_3 \times JD + g_3 \quad (8)$$

$$T_{air} = a_4 \times LST_{AD} + b_4 \times Z + c_4 \times SZ + d_4 \times Lon + e_4 \times Lat + f_4 \times JD + g_4 \quad (9)$$

where SZ is solar zenith; Lon is longitude; Lat is latitude; *JD* is Julian day; and a_1, a_2, …, g_3, and g_4 are regression coefficients. The multiple linear regression is the most common method for air temperature estimation using satellite-based LST because it has simple concept and is easy to use (Benali et al., 2012; Cristobal et al., 2008; Y. M. Xu et al., 2012). Apart from the simple multiple linear regression model, some complex models that are typically considered as machine-learning or data-mining methods such as the neural network (Zhao et al., 2007), the M5 model tree (Emamifar et al., 2013), and the random forests (Y. Xu et al., 2014) are also employed. A comparison among six types of statistical models indicates that there is little difference between the performances of simple and complex models for most cases (H. Zhang, Zhang, Ye, et al., 2016).

Taking the *T*air estimated from MODIS LST of the target CMA station and its neighboring stations as input, the corresponding 12 sets (4 types of MODIS LST × 3 types of *T*air) of TLR_{TEM} values were all derived using equation (1). For an independent validation, the regression equations (6)–(9) for the *T*air estimation of each target CMA station and its neighboring stations were trained using samples from all the CMA stations excluding the target CMA station and its neighboring stations, for example, when calculating the TLR_{TEM} for station no. 6, the samples for building and training the regression equations for estimating *T*air of station no. 6 and its neighboring stations would not include the samples from station no. 6 and its neighboring stations (i.e., station nos. 4, 5, 10, 11, 15, and 18).

3.2. Evaluating Methods

The performances of both the DFM and TEM methods were evaluated by comparisons between the MODIS LST-estimated TLR (TLR_{DFM} and TLR_{TEM}) and $TLR_{station}$. The monthly mean TLRs during 2003–2010 were calculated for each station, considering the limited number of available MODIS observations and the fact that monthly TLRs are the most popularly used (Immerzeel et al., 2014; F. Zhang et al., 2015). This resulted in each station having 12 monthly TLRs, which can be used for accuracy assessments. The root-mean-square deviation (RMSD) and the Pearson correlation coefficient (*R*) were selected as performance measurements. Comparisons were conducted for all three types of daily *T*air (*T*min, *T*max, and *T*mean). The type of *T*air with the highest accuracies was analyzed further. In addition, a number of potential factors, including the max distance, altitude, longitude, latitude, precipitation, sunshine duration, air temperature, vapor pressure, wind speed, and relative humidity, were analyzed for both DFM and TEM.

3.3. Evaluating the Effects of MODIS LST-Estimated TLR on Interpolating *T*air

The MODIS LST-estimated monthly TLRs based on both the DFM (TLR_{DFM}) and the TEM (TLR_{TEM}) methods were used for predicting *T*air at each station. The interpolation schemes are the following: all the *T*air data of neighboring stations are corrected to the height of target location using the TLR; all the corrected values were interpolated to the target location using the IDW (inverse distance weighted) method (Jarvis & Stuart, 2001). This is a very common method for interpolating *T*air based on the TLR (Stahl et al., 2006; L. Zhang et al., 2013). The interpolated *T*air values were compared to the observed *T*air values, and the RMSDs were computed as performance measurements. Further, the results from using TLR_{DFM} and TLR_{TEM} were compared with the results from using $TLR_{station}$ values to evaluate the effects of errors deduced by

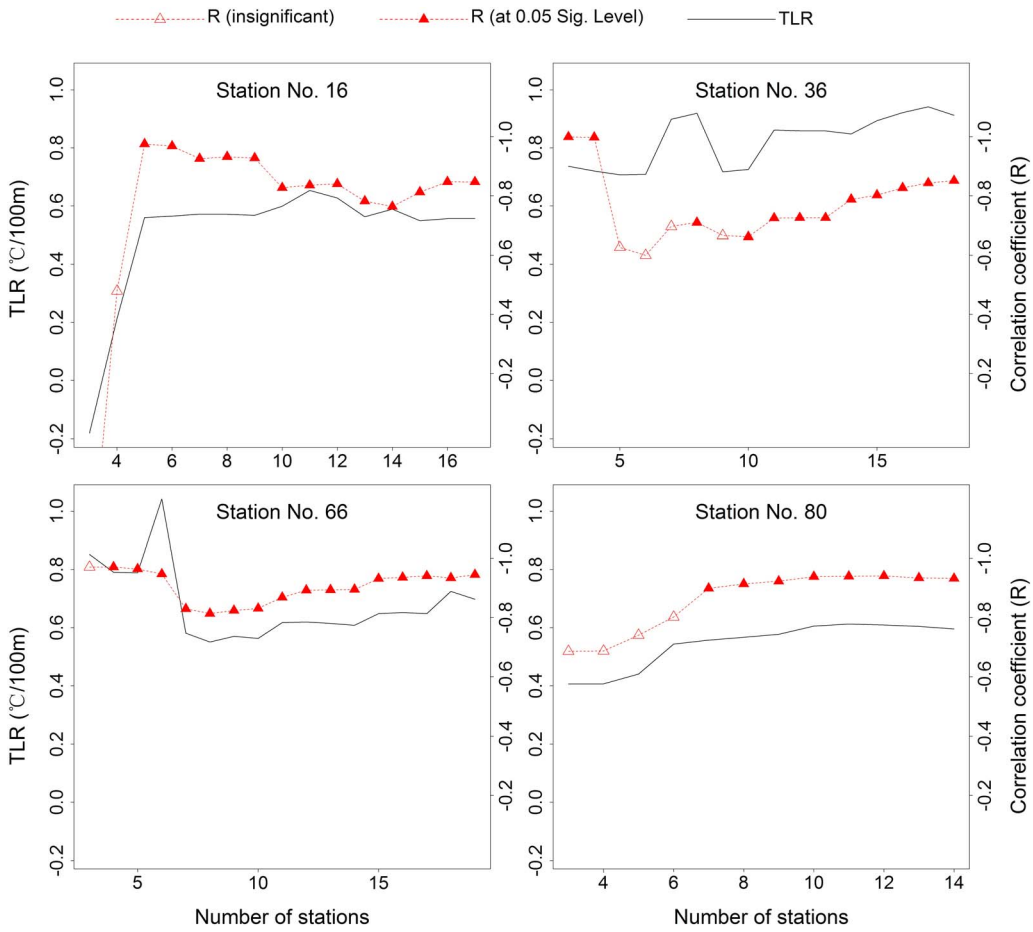

Figure 3. Sensitivity tests on the number of neighboring stations for temperature lapse rate (TLR) regression.

different methods. Lastly, uncertainties related to data availability (cloud contamination), MODIS LST combinations and interpolation schemes were investigated.

4. Results and Discussions

4.1. $TLR_{station}$

4.1.1. Sensitivity Tests on the Number of Neighboring Stations for TLR Regression

The sensitivity tests on the number of stations for evaluating the TLR regression at representative stations (Figure 3) showed that there were primarily three scenarios: (1) A relatively low *R* value (e.g., station no. 80) or even an exceptionally low *R* value (e.g., station no. 16) was obtained at the beginning of the evaluation and the *R* value increased gradually until reaching the 0.05 significance level; (2) a high *R* value was obtained at the beginning but it did not reach the 0.05 significance level until the station number increased to a sufficiently large value (e.g., station no. 66); and (3) the initial TLR already had a sufficiently high *R* value that reached the 0.05 significance level, whereas the *R* value might decrease when the station number increased (e.g., station no. 36). Lastly, the average number of selected neighboring stations for the TLR regression across all 86 stations was 5 ± 2 (mean ± standard deviation) and the mean max distance was 156 ± 50 km. The max number of selected neighboring stations is 11 with the max distance of 229 km.

4.1.2. Comparisons of $TLR_{station}$ for *T*mean, *T*min, and *T*max

The average $TLR_{station}$s for *T*mean (TLR_{Tmean}), *T*min (TLR_{Tmin}), and *T*max (TLR_{Tmax}) of all the 86 stations are obtained, which are 0.73 ± 0.24, 0.71 ± 0.24, and 0.78 ± 0.28 °C/100 m, respectively. Previous studies show that TLR_{Tmax} is generally larger than TLR_{Tmin}, and TLR_{Tmean} falls between them (Bolstad et al., 1998; Minder et al., 2010; Pepin, 2001; Rolland, 2003). Our result also reveals the same relative relationship, though three

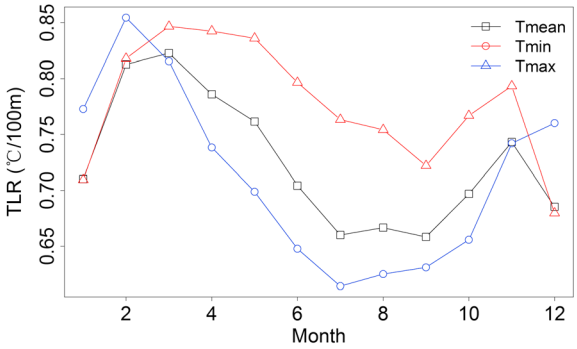

Figure 4. Monthly variation of average $TLR_{station}$ values of all the 86 stations for *T*mean, *T*min, and *T*max at all 86 stations. TLR = temperature lapse rate.

of them are, in fact, very close with one another. This is consistent with the results observed in central Himalayas (Kattel et al., 2013).

4.1.3. Monthly Variation of $TLR_{station}$

The average $TLR_{station}$s of all the 86 stations show strong monthly variation that it presents a double-humped pattern for all the three types of *T*air (Figure 4). For example, TLR_{Tmean} has the first peak in March and the second in November. This result is highly consistent with several previous studies from the TP (Kattel et al., 2013; X. Li et al., 2013; Yang et al., 2011). The amplitude of variation is as large as about 0.2 °C/100 m, which is also consistent with findings in the same region (Kattel et al., 2013; X. Li et al., 2013) as well as those in regions outside of the TP (Bolstad et al., 1998; Minder et al., 2010; Rolland, 2003). Due to the possibly strong variation of TLR in seasonal scales, several modeling studies have identified that monthly TLR is more reasonable than the annual one and improves hydrological simulation results (Immerzeel et al., 2014; F. Zhang et al., 2015). This study thus analyzed and verified the monthly TLRs afterward.

4.1.4. Spatial Distribution of $TLR_{station}$ and the Factors

Given that TLR_{Tmean} is the most commonly used parameter, only the spatial characteristics of $TLR_{station}$ for *T*mean are analyzed subsequently (Figure 5). It is evident that TLR_{Tmean} has a strong spatial variation. Previous studies (Kattel et al., 2013; X. Li et al., 2013; Marshall et al., 2007; Pepin, 2001; Yang et al., 2011) indicate that the TLR may be affected by humidity, air temperature, cloud cover, wind speed, and radiative and terrain conditions. The correlation analysis of 10 possible factors in this study indicates that TLR_{Tmean} may be influenced by altitude, longitude, precipitation, sunshine duration, vapor pressure, and humidity in the study area (Figure 6). Rising air tends to cool more slowly when air condensation occurs. Humidity is considered to be the main factor affecting the variation of the TLR for this region (Kattel et al., 2013; X. Li et al., 2013; W. Liu et al., 2013). This study confirms that TLR_{Tmean} has strongly negative correlations with relative humidity (−0.42) and vapor pressure (−0.38), suggesting that the calculated TLR_{Tmean} values could be reasonable. TLR_{Tmean} also shows a significantly positive correlation (0.34) with altitude. W. Liu et al. (2013) found that lower altitudes produced larger TLRs than higher altitudes in the northern slope of the central Himalayas and it largely depended on actual local conditions. The opposite results from those of this study can be explained by the decreasing water vapor with increasing altitude because altitude has a significantly negative correlation (−0.52) with vapor pressure. Clouds can reduce the TLR_{Tmean} by decreasing solar radiation and cooling the land surface (Yang et al., 2011). Due to the absence of cloudiness observations, precipitation and sunshine duration were used as alternatives here. Our results indicated that longer sunshine duration and less precipitation, indicating less cloudiness, could result in higher TLR_{Tmean} values. The strongly negative correlation (−0.39) between longitude and TLR_{Tmean} may be largely because the altitude decreases and the air becomes moist in an eastward direction toward the edge of the TP. It may be noteworthy that wind speed did not indicate a significant correlation with TLR_{Tmean}, but its effects might fluctuate with the integration of other factors such as humidity and altitude, etc.

4.1.5. The Reliability of $TLR_{station}$

Previous studies (Rolland, 2003) indicate that local conditions play an important role in the TLR. An efficient scheme was thus applied as described in section 3.1.1, which took a full consideration of locality. Since $TLR_{station}$ is considered as the observed TLR in this study, its reliability is crucial. To validate the $TLR_{station}$ values, the *T*mean interpolation accuracies were computed and a sensitivity test was conducted as follows: The *T*mean interpolation accuracies were initially computed based on the original TLR_{Tmean} values for each CMA station. Then, seven rounds of sensitivity tests were conducted for each station. For each round another 0.1 °C/100 m was added to the original TLR_{Tmean} values and the *T*mean interpolation accuracies were calculated. After the seven rounds of testing were completed, the TLR_{Tmean} values were set to the original TLR_{Tmean} values and another similar seven rounds of

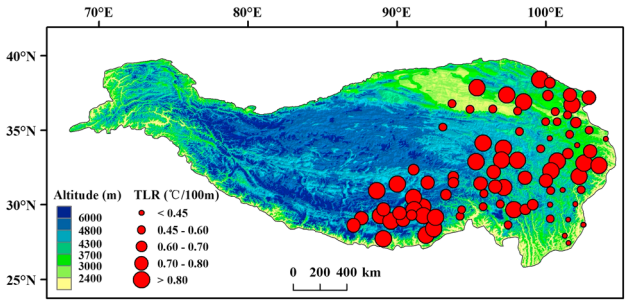

Figure 5. Spatial distribution of $TLR_{station}$ for *T*mean across the Tibetan Plateau. TLR = temperature lapse rate.

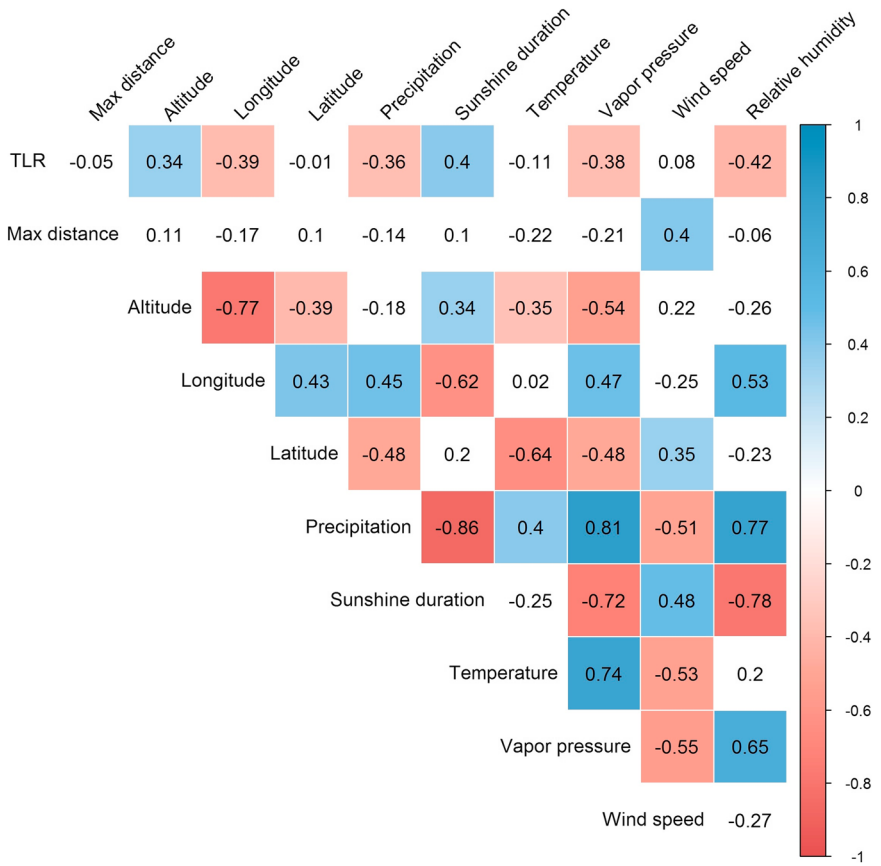

Figure 6. Correlation matrix of $TLR_{station}$ for *T*mean, max distance, altitude, longitude, latitude, precipitation, sunshine duration, air temperature, vapor pressure, wind speed, and relative humidity. Significantly (at 0.01 significance level) positive correlation values are shown in blue; significantly (at 0.01 significance level) negative correlation values are shown in red; insignificant correlation values are filled as blank. TLR = temperature lapse rate.

sensitivity tests were conducted with a decrease of 0.1 °C/100 m for each round. The results are shown in Figure S1. For the total 15 rounds, the RMSDs ranged from 1.52 to 2.90 °C and the original TLR_{Tmean}s values indicate the highest accuracies. This further indicates that the calculation method described in section 3.1.1 could produce reasonable TLRs that were representative of the observed TLRs in general.

4.2. MODIS LST-Estimated TLR

4.2.1. Accuracy Assessment for TLR_{DFM} and TLR_{TEM}

As shown in Figure 7, it is clear that the MODIS LST-estimated TLR is more accurate for *T*mean than for *T*min and *T*max in comparison to $TLR_{station}$ that is designated as the observed or true TLR. This is true under all scenarios, including the four different MODIS LST terms and the DFM and TEM methods. The DFM method produces the best accuracies for TLR_{Tmean}, with a mean RMSD of 0.40 °C/100 m versus 0.43 and 0.44 °C/100 m for TLR_{Tmin} and TLR_{Tmax}, respectively. Similarly, the TEM method produces the best TLR_{Tmean} estimation (mean RMSD: 0.24 °C/100 m), followed by TLR_{Tmin} (0.26 °C/100 m) and TLR_{Tmax} (0.27 °C/100 m). Given that TLR_{Tmean} is the most commonly used parameter, additional results are focused on TLR_{Tmean}.

The accuracies of the TLR estimation based on different MODIS LST terms are notably different (Figure 7). For both DFM and TEM, cases using MODIS daytime LSTs indicate noticeably lower accuracies than those using MODIS nighttime LSTs. For DFM, the averaged RMSDs for cases using MODIS daytime and nighttime LSTs are 0.60 and 0.21 °C/100 m, respectively. The accuracies are much lower than those by Mutiibwa et al. (2015), which is mainly because their study compared the lapse rates of instantaneous *T*air with those of MODIS LSTs, whereas this study compared the daily values. For TEM, the differences of TLR estimation based on MODIS daytime and nighttime LSTs are small with averaged RMSDs of 0.30 and 0.19 °C/100 m,

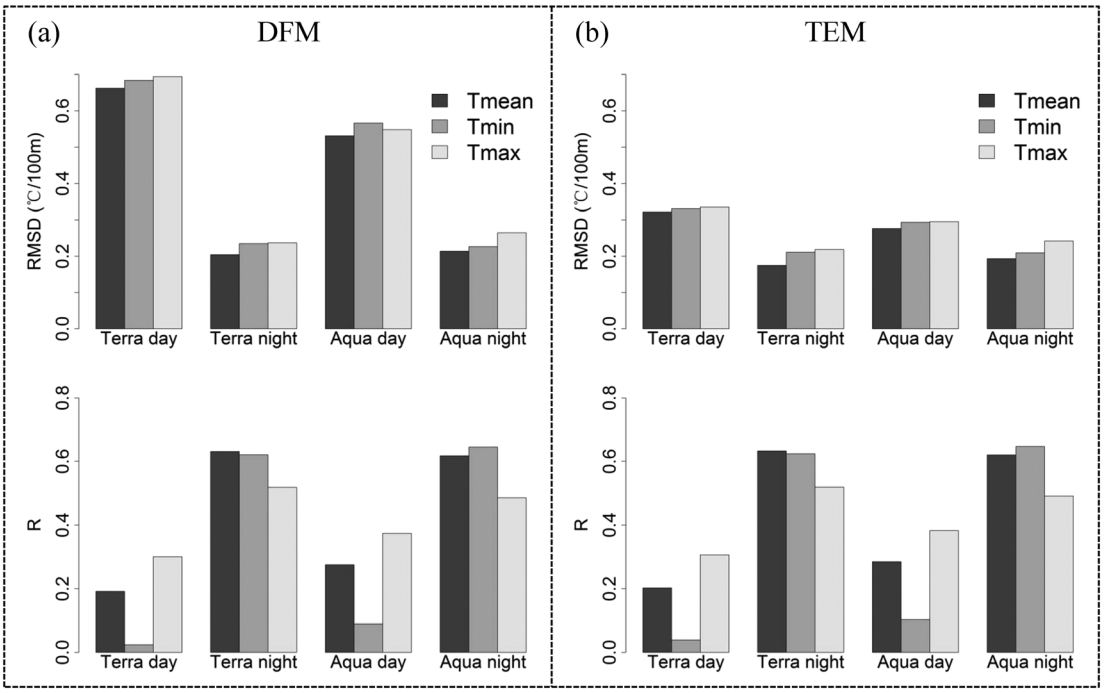

Figure 7. Accuracies of the directly from Moderate Resolution Imaging Spectroradiometer TLR (DFM) (a) and temperature estimation from Moderate Resolution Imaging Spectroradiometer TLR (TEM) (b) methods for TLR estimation for *T*mean, *T*min and *T*max in comparison to $TLR_{station}$. TLR = temperature lapse rate; RMSD = root-mean-square deviation.

respectively. In summary, MODIS nighttime LSTs are better for TLR estimation using both DFM and TEM with mean RMSDs of 0.21 and 0.19 °C/100 m, respectively.

4.2.2. Spatial and Temporal Uncertainties of TLR_{DFM} and TLR_{TEM}

The spatial distributions of the RMSDs for the MODIS LST-estimated TLR compared to the $TLR_{station}$ are shown in Figure 8. For cases based on the MODIS daytime LST (Figures 8a and 8c), the spatial patterns of accuracies from DFM and TEM are distinct. During daytime, uncertainty mainly fluctuates with the relationship between

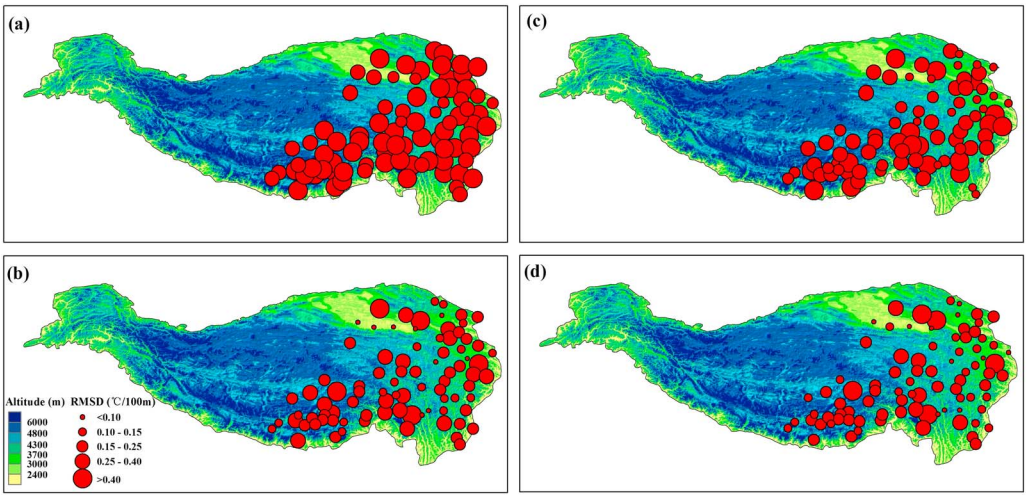

Figure 8. Spatial distribution of root-mean-square deviations (RMSDs) for TLR_{DFM} from Moderate Resolution Imaging Spectroradiometer daytime (a) and nighttime (b) land surface temperature (LST), and for TLR_{TEM} from Moderate Resolution Imaging Spectroradiometer daytime (c) and nighttime (d) LST compared to $TLR_{station}$. TLR = temperature lapse rate.

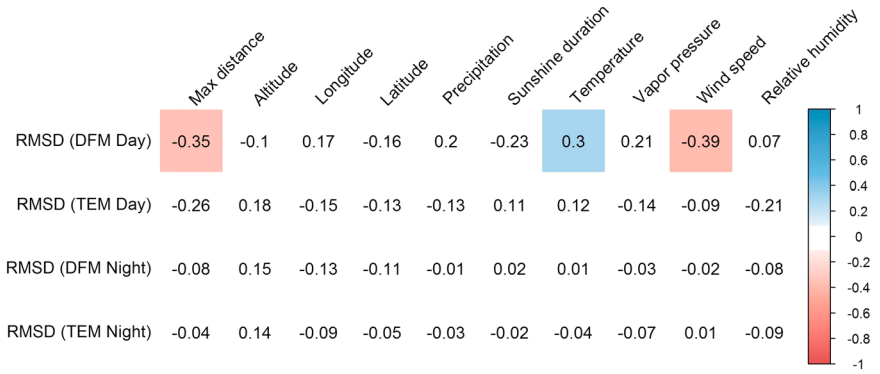

Figure 9. Correlation analysis between the accuracies of Moderate Resolution Imaging Spectroradiometer (MODIS) land surface temperature-estimated TLR_{Tmean} and local climatic/terrain conditions. Significantly (at 0.01 significance level) positive correlation values are shown in blue; significantly (at 0.01 significance level) negative correlation values are shown in red; insignificant correlation values are filled as blank. TLR = temperature lapse rate; RMSD = root-mean-square deviation; DFM = directly from MODIS TLR; TEM = temperature estimation from MODIS TLR.

*T*air and LSTs impacted by solar radiation, clouds, or hill shadows (Benali et al., 2012; W. Wang et al., 2008; H. Zhang, Zhang, Zhang, et al., 2016). For DFM, a number of factors, including the max distance, air temperature, and wind speed, seem to have effects on the accuracies of cases based on the MODIS daytime LST (Figure 9). Generally, solar heating warms the land surface to produce the temperature lapse between the LST and *T*air during daytime. Strong solar heating (air temperature) may introduce uncertainties to disturb the balance between *T*air and LSTs. However, strong winds can play a neutralizing role by facilitating heat mixing to decrease the uncertainties caused by clouds or mixed-pixel effects (Hall, Box, et al., 2008). The max distance may be related to data quality because the MODIS daytime LST becomes more spatially representative with greater values of the max distance. Many studies reported that MODIS daytime LSTs have more problems in pixel heterogeneity than MODIS nighttime LSTs (W. Wang et al., 2008; H. Zhang, Zhang, Zhang, et al., 2016). Thus, the DFM method based on MODIS daytime LSTs produced very low accuracies due to various uncertainty sources. Compared with DFM, the accuracies of cases using TEM based on MODIS daytime LSTs are found to have no significant correlation with any of the factors (Figure 9). This may be due to the fundamental difference between the two methods: TLR_{TEM} is calculated from the *T*air estimated using MODIS LSTs, whereas TLR_{DFM} is calculated directly from MODIS LSTs. The factors affecting the performance of TEM may be more relevant with those affecting the accuracies of *T*air estimations. Because the MODIS daytime LST is not as strong a predictor as the MODIS nighttime LST for *T*air estimation (Oyler et al., 2016; W. Zhang et al., 2011; H. Zhang, Zhang, Ye, et al., 2016), the effects of factors affecting the *T*air-LST relationship may be smoothed by other variables, such as elevation, longitude, and Julian day.

It is obvious that the accuracies from cases using the MODIS daytime LST are clearly lower than those using MODIS nighttime LST for almost all the 86 stations (Figure 8). Compared with MODIS daytime LSTs, the complexity is largely reduced for cases based on MODIS nighttime LSTs. At night, the variation of MODIS LSTs agrees noticeably well with that of *T*air (Pepin et al., 2016). Oyler et al. (2016) also found that the spatial patterns of nighttime LSTs were more similar to *T*air than those of daytime LST. In this study, no meteorological factor was found to have a substantial influence on the accuracies of cases using MODIS nighttime LST for either DFM or TEM (Figure 9). In addition, MODIS nighttime LSTs have been widely identified as indicators of notably higher performance in *T*air estimations than MODIS daytime LSTs (Benali et al., 2012; W. Zhang et al., 2011; H. Zhang, Zhang, Ye, et al., 2016). The spatial patterns of accuracies of the TLRs using DFM and TEM based on MODIS nighttime LSTs are consistent (Figures 8b and 8d), and they both show obviously higher accuracies than those based on MODIS daytime LSTs.

Monthly accuracies for cases using Terra nighttime LSTs indicate that both the DFM and TEM methods have lower accuracies in warmer seasons and higher accuracies in colder seasons (Figure S2). This may be explained by the stronger influences of land cover in warmer seasons due to the absence of snow cover. TEM outperforms DFM for all months with the largest differences in RMSDs of 0.04 °C/100 m for the TLR estimation in comparison with $TLR_{station}$ occurring in January, February, March, May, and December. It should be

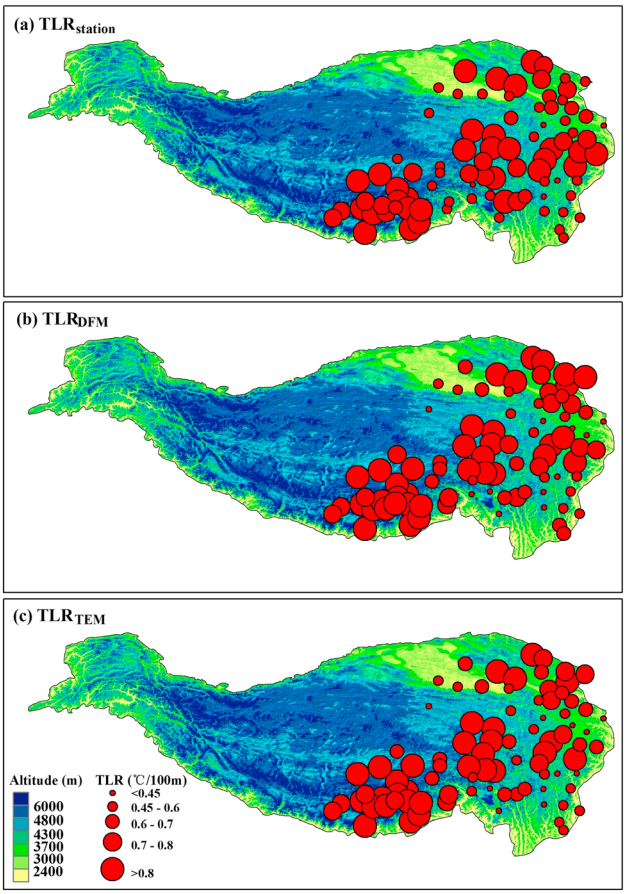

Figure 10. Spatial distributions of TLR$_{Tmean}$ values derived from (b) directly from MODIS LST (DFM) and (c) temperature estimation from MODIS LST (TEM) based on Terra nighttime LSTs, and those based on station (a). LST = land surface temperature.

noted that the largest RMSD difference (i.e., 0.04 °C/100 m) may produce a relatively small error of 0.4 °C on average for *T*air prediction.

4.2.3. Evaluation of Spatial and Temporal Patterns of TLR$_{DFM}$ and TLR$_{TEM}$

Figure 10 plots the TLR$_{DFM}$, TLR$_{TEM}$, and TLR$_{station}$ of *T*mean for all 86 stations. The spatially averaged values (mean ± standard deviation) for all the stations are 0.76 ± 0.25, 0.71 ± 0.22, and 0.74 ± 0.24 °C/100 m for TLR$_{DFM}$, TLR$_{TEM}$, and TLR$_{station}$, respectively. Both TLR$_{DFM}$ and TLR$_{TEM}$ seem to have spatial patterns similar to TLR$_{station}$, while the averaged RMSDs (Figure 7) indicate that the TEM method shows slightly better accuracies than the DFM method. The spatial distribution characteristics of TLR$_{station}$ are mainly controlled by local climatic and terrain conditions. Both TLR$_{DFM}$ and TLR$_{TEM}$ indicate relatively strong correlations with altitude, longitude, sunshine duration, and relative humidity (Figure 11). This is highly consistent with TLR$_{station}$, indicating that they have spatial patterns very similar to TLR$_{station}$. In addition, both the DFM and TEM methods captured the dynamics of monthly TLRs well (Figure S3), with almost the same high *R* value (0.88).

To conclude, both the spatial and temporal patterns of the MODIS LST-estimated TLR$_{Tmean}$ using both DFM and TEM are highly consistent with TLR$_{station}$. Thus, the capability for the two tested methods to reasonably reproduce the TLR$_{Tmean}$ has been verified.

4.3. How Much Does the TLR Derived From MODIS LSTs Affect the Accuracies of the *T*air Estimation?

Figure 12 shows that when estimating *T*air based on the TLR derived from the MODIS daytime LST, TEM produces notably better accuracy than DFM, with averaged RMSDs of 1.92 versus 2.66 °C. However, for cases based on the MODIS nighttime LST, TEM is only slightly better than DFM with averaged RMSDs of 1.70 versus 1.73 °C. In addition, both the TLR$_{DFM}$ and TLR$_{TEM}$ based on the MODIS nighttime LST show comparative accuracies to those using TLR$_{station}$ for the *T*air estimation (the averaged RMSD is 1.61 °C). The monthly accuracy variations are shown in Figure S4, and it is clear that both TLR$_{DFM}$ and TLR$_{TEM}$ show a very similar seasonal pattern to that of TLR$_{station}$ with higher accuracies in summer and lower accuracies in winter. This finding is also consistent with that from the central Himalayas (Kattel et al., 2013).

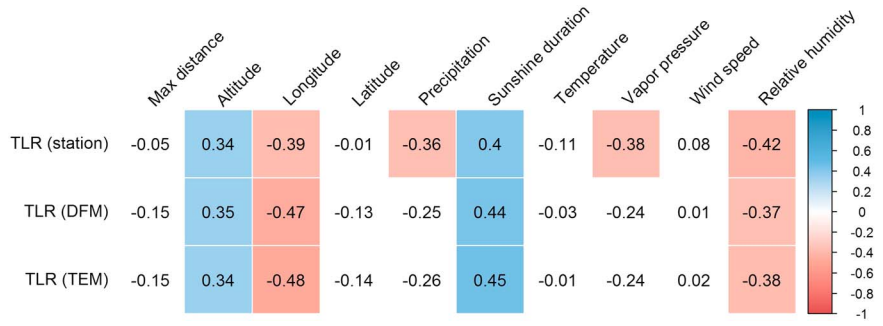

Figure 11. Correlation analysis between local climatic/terrain conditions and the three types of temperature lapse rate (TLR), including TLR$_{station}$, TLR$_{DFM}$, and TLR$_{TEM}$. Significantly (at 0.01 significance level) positive correlation values are shown in blue; significantly (at 0.01 significance level) negative correlation values are shown in red; insignificant correlation values are filled as blank.

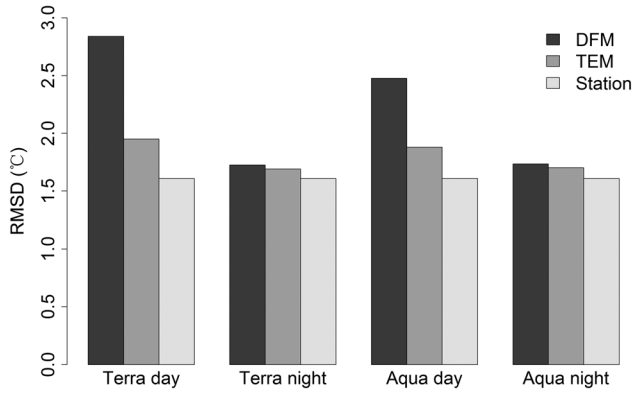

Figure 12. The *T*air interpolation accuracies using the estimated TLR_{Tmean} from directly from MODIS LST (DFM) and temperature estimation from MODIS LST (TEM) based on different MODIS LST terms. TLR = temperature lapse rate. MODIS = Moderate Resolution Imaging Spectroradiometer; LST = land surface temperature; RMSD = root-mean-square deviation.

Though the differences in the *T*air interpolation accuracy among three of them seem to be small, it should be noted that the effects of the TLR primarily depend on the "elevation difference." The influence of the TLR becomes greater as the difference in altitude between the target station and the neighboring stations increases. Here we defined the "sensitivity" as the averaged absolute variation of interpolated *T*air for every change of 0.1 °C/100 m in the TLR. The sensitivity of the interpolated *T*air accuracy to the variation of $TLR_{station}$ for all 86 CMA stations was thus calculated using the same variation range as that in section 4.1.3. The results show that there is a very high positive correlation (0.93) between the sensitivity to the TLR and the elevation differences (Figure S5). A "reference" altitude difference is needed to evaluate the average condition. In this study, this value was set to 1,000 m, which was approximately the difference between the mean elevation of all CMA stations in the TP (~3,300 m) and the mean elevation of the TP (~4,300 m) based on the data set from the Shuttle Radar Topography Mission. In other words, we have to predict the *T*air of a location at an elevation of approximately 4,300 m using the TLR and the *T*air data from CMA stations at elevations of approximately 3,300 m on average. Then, multiplying the error of the estimated TLR by the reference altitude difference (1,000 m) will produce the expected error of the interpolated *T*air deduced by the TLR estimation. Lastly, it can be concluded that using TEM and DFM based on the MODIS nighttime LST and with averaged RMSDs of 0.19 and 0.21 °C/100 m, respectively, are expected to generally produce errors for *T*air interpolation at 1.9 and 2.1 °C in the TP, respectively. Since the errors are generally ~2 °C for daily *T*air estimation in high mountain areas based on remote sensing products and climate reanalysis data sets (H. Zhang, Zhang, Ye, et al., 2016; Zhou et al., 2017), the *T*air interpolation accuracies from using the MODIS-estimated TLR are considered to be acceptable for daily *T*air estimation in the TP. However, the accuracies of the MODIS-estimated TLR may not be accepted for climatic analysis considering that the climatic warming rates are generally less than 0.1 °C/year for the TP (X. Liu & Chen, 2000).

For practical application, the DFM method may be more useful because it does not need actual local *T*air observations, whereas the TEM method relies on *T*air estimation using statistical methods. DFM may be particularly important for its potential use in downscaling *T*air data from large-scale climatic forcing data sets, such as the Global Land Data Assimilation System and the China Meteorological Forcing Dataset.

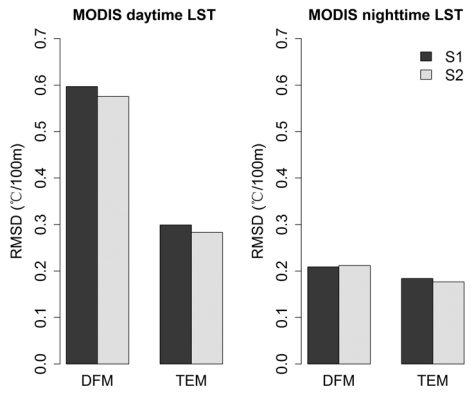

Figure 13. Comparisons of accuracies from the situations of S1 and S2 using the directly from MODIS LST (DFM) and temperature estimation from MODIS LST (TEM) methods for temperature lapse rate estimation, based on MODIS daytime (left) and nighttime (right) LST. MODIS = Moderate Resolution Imaging Spectroradiometer; LST = land surface temperature. RMSD = root-mean-square deviation.

4.4. Cloud Contamination and Data Quality

Satellite-based LST data are often contaminated by cloud cover (Z.-L. Li et al., 2013). Clouds may generally affect the TLR estimation based on MODIS LST in two ways: (1) cloud cover can greatly decrease the number of available LST data (Benali et al., 2012; H. Zhang, Zhang, Ye, et al., 2016); (2) undetected clouds may introduce errors in LST data due to the deficiency of cloud detection algorithm applied in MODIS product (Ackerman et al., 1998; H. Zhang, Zhang, Zhang, et al., 2016).

High cloud cover fractions are widely reported in the TP (Tang et al., 2013; Yu et al., 2016), and the average cloud cover rate is as high as 35–54% for the four MODIS LST terms during 2003–2010 (H. Zhang, Zhang, Ye, et al., 2016). For the MODIS LST pixels used in this study, the averaged cloud contamination rates are 45.3, 45.1, 51.8, and 40.6% for Terra daytime, Terra nighttime, Aqua daytime, and Aqua nighttime LST terms, respectively. As an indirect effect of cloud contamination, the constraint employed here that only days with four available LST terms are used can further decrease the available LST data, and for this study the days satisfying this criteria only account for 23.7% of the whole

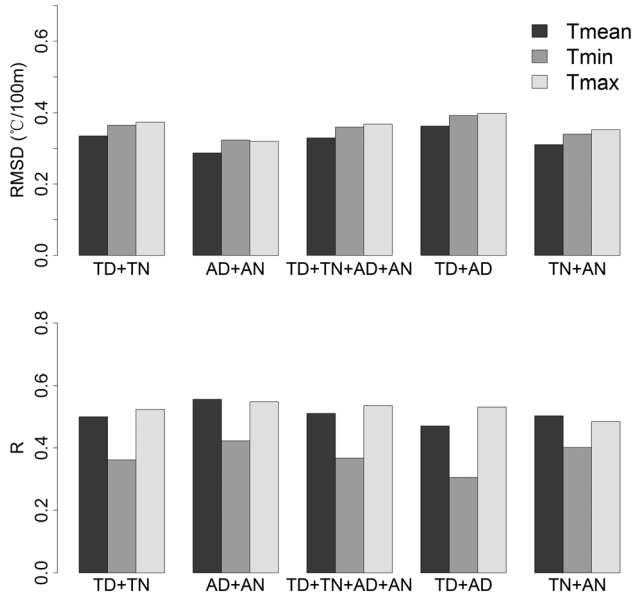

Figure 14. Accuracies of the directly from Moderate Resolution Imaging Spectroradiometer land surface temperature method based on different combinations of Moderate Resolution Imaging Spectroradiometer land surface temperature terms. RMSD = root-mean-square deviation.

study period. To alleviate this problem, the multiyear average, monthly TLRs are used for this study resulting that for each month at each station there is ~60 clear days that can be used for TLR calculation.

However, the large proportion of missing data due to cloud cover may lead to a bias for studies using MODIS LST (Hall et al., 2006; Hall, Williams, et al., 2008). It should be noted that in this study, though only days with four available MODIS LST terms were used for calculating the TLR_{DFM} and TLR_{TEM}, the $TLR_{station}$ is derived using the whole study period including both clear and cloudy days. To further evaluate the representativeness of estimated TLRs and the feasibility of our methods, two situations related with cloud cover are defined as follows: (1) only days with four MODIS observations without cloud coverage are used, referred to as "S1"; and (2) for each MODIS LST term, all the days with corresponding LST term data available are used, referred to as "S2." The detailed information of the four cases are listed in Table S1. Figure 13 shows the comparison results of the two situations. For cases using MODIS daytime LST, the accuracies of situation S2 are slightly higher than that of situation S1 with a small decrease of RMSD of ~0.02 °C/100 m. And the accuracies of both situations are almost the same for cases using MODIS nighttime LST with the difference in RMSD of less than 0.01 °C/100 m. This indicates that the missing data caused by cloud coverage seem to have limited effect in our study. This is possibly owing to that the calculated TLRs in this study are multiyear average, monthly TLRs resulting in sufficient samples for calculation. In addition, the averaged $TLR_{station}$ values from days with four available MODIS LST terms are 0.74, 0.72, and 0.82 °C/100 m for *T*mean, *T*min, and *T*max, respectively, which are well consistent with those of 0.73, 0.71, and 0.78 °C/100 m from the whole period (see section 4.1.1), respectively. This also supports that for estimating the multiyear average, monthly TLRs, the representativeness of the selected days did not decrease greatly with the large proportion of missing data. We also did a correlation analysis between the accuracies (RMSD) and cloud cover rates among the 86 stations and no significant correlation was found for either of the two situations.

The data quality of MODIS LST may be affected by undetected clouds, especially for MODIS nighttime LST (Ackerman et al., 1998; H. Zhang, Zhang, Zhang, et al., 2016). Though the LST data with the lowest data quality (i.e., with the data quality flag value of 3) have been removed as mentioned before, undetected clouds may still exist in the MODIS nighttime LST. Based on the comprehensive analysis using ground observations in combination with MODIS LST data, H. Zhang, Zhang, Zhang, et al. (2016) find that using the days with all four available MODIS LST observations can greatly filter out pixels with undetected clouds, and this is actually the same way as situation S1 employed in this study. It is hard to distinguish and eliminate the mixed effects of undetected clouds and the missing data caused by cloud contamination. However, the comparison between the two situations related with different conditions of cloud coverage shows their accuracies are similar and both acceptable (Figure 13), indicating that both DFM and TEM using MODIS nighttime LST are feasible to estimate the multiyear average, monthly TLRs for the TP with acceptable accuracies during the study period.

4.5. Other Uncertainties in TLR_{DFM} and TLR_{TEM}

Combinations of MODIS LST terms may have different effects on the results from the two fundamentally different methods. Since TEM is based on *T*air estimation, improving *T*air estimation accuracies from MODIS LSTs may contribute to more accurate TLR estimations. More MODIS LST terms have been utilized in other studies to improve the *T*air estimations (Benali et al., 2012; W. Zhang et al., 2011; H. Zhang, Zhang, Ye, et al., 2016). However, it is found that when a MODIS nighttime LST term is used, adding more nighttime or daytime LST terms has very little effect on the accuracies (H. Zhang, Zhang, Ye, et al., 2016). Multiple MODIS terms were thus not considered for the TEM method in this study. For DFM, the effects of LST combinations remained unknown. We tested the performances of DFM based on five different combinations of MODIS LSTs (Figure 14). The results are fully consistent with section 4.2.1 that TLR_{Tmean} estimations are always more accurate than TLR_{Tmin} and TLR_{Tmax} for all five combinations. The lowest averaged RMSD for TLR_{Tmean} based on the

combination of Aqua day and Aqua night is only 0.29 °C/100 m. This indicates that adding more LST terms for DFM generally resulted in even lower accuracies than the one based on a single MODIS nighttime LST term with a lower RMSD of 0.21 °C/100 m. It may also indicate that simply combing multiple LST terms cannot take full advantage of LST observations at different pass times but add more uncertainties instead. Daily mean LST may be more representative for estimating daily *T*air and the TLR, but its calculation requires that all the four MODIS LST terms are available (Duan et al., 2012), which could greatly decrease the data amounts as shown in Table S1. Future studies may develop more efficient algorithms to take the full advantage of the four daily MODIS instantaneous observations for better TLR estimation.

The interpolation scheme may be another uncertainty source. In previous studies that used the TLR for the TP (Immerzeel et al., 2014; L. Zhang et al., 2013; F. Zhang et al., 2015), there are two main types of interpolation schemes: (1) one scheme uses multiple neighboring stations and typically needs to employ a weight calculating method such as the IDW, similar to the interpolation scheme used in this study; and (2) the other scheme only uses a single nearest station and interpolates *T*air directly based on the TLR. The first type of interpolation scheme is mainly used for areas with relatively dense station coverage (Immerzeel et al., 2014) or for large-scale research (L. Zhang et al., 2013). It should be noted that there are some other types of weight calculating methods apart from IDW, such as the Gaussian filter and Kriging, and they are found to have similar performances for interpolation methods using the TLR (Stahl et al., 2006). The second type of interpolation scheme is typically applied in midsized or small basins with only one station which is very common in the TP (H. Gao et al., 2012; F. Zhang et al., 2015). The TLR is inevitably crucial for the second scheme but the importance of the TLR is questionable for the first one due to the process of weight calculation. Sensitivity tests as specified in section 4.3 show that a 0.1 °C/100 m change in the $TLR_{station}$ is found to result in the *T*air changes of 0.32 and 0.38 °C on average for the first and second types of schemes, respectively. As previously discussed, the effects of the TLR on *T*air interpolation mainly depend on the altitude difference. The averaged altitude differences for the two schemes are 356 and 381 m, respectively, which are expected to generally produce changes of 0.36 and 0.38 °C, respectively, for every change of 0.1 °C/100 m in the TLR. The small difference between 0.36 and 0.32 °C for the first scheme indicates that the weight calculation process truly compensates for some effects of the TLR, but the TLR still plays a dominant role in the first type of scheme.

5. Conclusion

Our research investigated and compared two methods of estimating the air TLR based on MODIS LSTs. The observed TLRs were derived from neighboring stations selected through sensitivity tests among the 86 CMA stations located in the eastern TP. Both the method that computes lapse rates directly from MODIS (DFM) LSTs and the method based on air temperature estimation from MODIS LSTs (TEM) were applied for estimating the monthly mean TLR of daily maximum (*T*max), minimum (*T*min), and mean (*T*mean) air temperatures. In addition, all four MODIS LST terms, including Terra day, Terra night, Aqua day, and Aqua night LSTs, were tested using both methods.

The results show that based on MODIS LST, the TLR of *T*mean is more accurately estimated than that of *T*min and *T*max. This finding is consistent among the two methods of DFM and TEM using the four MODIS LST terms. For cases based on MODIS daytime LSTs, TEM indicates notably higher accuracies than DFM, with averaged RMSDs of 0.30 for TEM versus 0.60 °C/100 m for DFM. However, for those cases based on MODIS nighttime LSTs, both DFM and TEM show obviously higher performances with averaged RMSDs of 0.21 and 0.19 °C/100 m, respectively. Such errors in the TLR are expected to result in the *T*air interpolation errors of 2.1 and 1.9 °C on average based on DFM and TEM, respectively. The spatial and seasonal patterns of MODIS LST-estimated TLR_{Tmean} are highly consistent with those of $TLR_{station}$ for both DFM and TEM.

This study provides a useful implication that directly computing the lapse rates of MODIS nighttime LSTs has the capability to simulate the monthly TLR_{Tmean} at relatively high accuracies. It can help alleviate the data-sparse problem in downscaling *T*air or hydrological modeling studies in ungauged areas. The DFM method also has a good potential to be applied in the western TP with extremely sparse observations due to its advantage of needing no *T*air observations compared with the TEM method. Considering the obviously different land covers, elevations, and climatic conditions, the performance of the DFM method on the western

TP may need further studies. It should be noted that either DFM or TEM is not unique for the TP, but future studies may be needed to evaluate their performances in other regions.

Acknowledgments
This study was supported by the National Natural Science Foundation of China (grants 41422101 and 41701079), International Partnership Program of Chinese Academy of Sciences (grant 131C11KYSB20160061), and China Postdoctoral Science Foundation (grant 2017M611013). The authors are grateful to the Chinese Meteorology Administration (http://data.cma.cn/) for providing air temperature data. The MODIS LST products can be downloaded at no charge from the Reverb website (http://reverb.echo.nasa.gov/).

References

Ackerman, S. A., Strabala, K. I., Menzel, W. P., Frey, R. A., Moeller, C. C., & Gumley, L. E. (1998). Discriminating clear sky from clouds with MODIS. *Journal of Geophysical Research*, *103*(D24), 32,141–32,157. https://doi.org/10.1029/1998JD200032

Arnold, N. S., Rees, W. G., Hodson, A. J., & Kohler, J. (2006). Topographic controls on the surface energy balance of a high Arctic valley glacier. *Journal of Geophysical Research*, *111*, F02011. https://doi.org/10.1029/2005JF000426

Benali, A., Carvalho, A. C., Nunes, J. P., Carvalhais, N., & Santos, A. (2012). Estimating air surface temperature in Portugal using MODIS LST data. *Remote Sensing of Environment*, *124*(0), 108–121. https://doi.org/10.1016/j.rse.2012.04.024

Bolstad, P. V., Swift, L., Collins, F., & Régnière, J. (1998). Measured and predicted air temperatures at basin to regional scales in the southern Appalachian mountains. *Agricultural and Forest Meteorology*, *91*(3–4), 161–176. https://doi.org/10.1016/S0168-1923(98)00076-8

Cai, D., You, Q., Fraedrich, K., & Guan, Y. (2016). Spatiotemporal Temperature Variability over the Tibetan Plateau: Altitudinal Dependence Associated with the Global Warming Hiatus.

Craney, T. A., & Surles, J. G. (2002). Model-dependent variance inflation factor cutoff values. *Quality Engineering*, *14*(3), 391–403. https://doi.org/10.1081/QEN-120001878

Cristobal, J., Ninyerola, M., & Pons, X. (2008). Modeling air temperature through a combination of remote sensing and GIS data. *Journal of Geophysical Research*, *113*, D13106. https://doi.org/10.1029/2007JD009318

Ding, B., Yang, K., Qin, J., Wang, L., Chen, Y., & He, X. (2014). The dependence of precipitation types on surface elevation and meteorological conditions and its parameterization. *Journal of Hydrology*, *513*(0), 154–163. https://doi.org/10.1016/j.jhydrol.2014.03.038

Dobrowski, S. Z., Abatzoglou, J. T., Greenberg, J. A., & Schladow, S. (2009). How much influence does landscape-scale physiography have on air temperature in a mountain environment? *Agricultural and Forest Meteorology*, *149*(10), 1751–1758. https://doi.org/10.1016/j.agrformet.2009.06.006

Dodson, R., & Marks, D. (1997). Daily air temperature interpolated at high spatial resolution over a large mountainous region. *Climate Research*, *8*(1), 1–20. https://doi.org/10.3354/cr008001

Duan, S.-B., Li, Z.-L., Wang, N., Wu, H., & Tang, B.-H. (2012). Evaluation of six land-surface diurnal temperature cycle models using clear-sky in situ and satellite data. *Remote Sensing of Environment*, *124*(0), 15–25. https://doi.org/10.1016/j.rse.2012.04.016

Emamifar, S., Rahimikhoob, A., & Noroozi, A. A. (2013). Daily mean air temperature estimation from MODIS land surface temperature products based on M5 model tree. *International Journal of Climatology*, *33*(15), 3174–3181. https://doi.org/10.1002/joc.3655

Fu, G., Shen, Z., Zhang, X., Shi, P., Zhang, Y., & Wu, J. (2011). Estimating air temperature of an alpine meadow on the northern Tibetan Plateau using MODIS land surface temperature. *Acta Ecologica Sinica*, *31*(1), 8–13. https://doi.org/10.1016/j.chnaes.2010.11.002

Gao, H., He, X., Ye, B., & Pu, J. (2012). Modeling the runoff and glacier mass balance in a small watershed on the central Tibetan Plateau, China, from 1955 to 2008. *Hydrological Processes*, *26*(11), 1593–1603. https://doi.org/10.1002/hyp.8256

Gao, T. G., Kang, S. C., Lan, C., Zhang, T. J., Guoshuai, Z. S., Yulan, Z. L., & Sillanpaa, M. (2015). Simulation and analysis of glacier runoff and mass balance in the Nam Co basin, southern Tibetan Plateau. *Journal of Glaciology*, *61*(227), 447–460. https://doi.org/10.3189/2015JoG14J170

Guo, X., Wang, L., & Tian, L. (2016). Spatio-temporal variability of vertical gradients of major meteorological observations around the Tibetan Plateau. *International Journal of Climatology*, *36*(4), 1901–1916. https://doi.org/10.1002/joc.4468

Hachem, S., Duguay, C. R., & Allard, M. (2012). Comparison of MODIS-derived land surface temperatures with ground surface and air temperature measurements in continuous permafrost terrain. *The Cryosphere*, *6*(1), 51–69. https://doi.org/10.5194/tc-6-51-2012

Hall, D. K., Box, J. E., Casey, K. A., Hook, S. J., Shuman, C. A., & Steffen, K. (2008). Comparison of satellite-derived and in-situ observations of ice and snow surface temperatures over Greenland. *Remote Sensing of Environment*, *112*(10), 3739–3749. https://doi.org/10.1016/j.rse.2008.05.007

Hall, D. K., Williams, R. S., Casey, K. A., DiGirolamo, N. E., & Wan, Z. (2006). Satellite-derived, melt-season surface temperature of the Greenland ice sheet (2000–2005) and its relationship to mass balance. *Geophysical Research Letters*, *33*, L11501. https://doi.org/10.1029/2006GL026444

Hall, D. K., Williams, R. S., Luthcke, S. B., & Digirolamo, N. E. (2008). Greenland ice sheet surface temperature, melt and mass loss: 2000–06. *Journal of Glaciology*, *54*(184), 81–93. https://doi.org/10.3189/002214308784409170

Hänninen, H., Zhang, G., Rikala, R., Luoranen, J., Konttinen, K., & Repo, T. (2013). Frost hardening of Scots pine seedlings in relation to the climatic year-to-year variation in air temperature. *Agricultural and Forest Meteorology*, *177*, 1–9. https://doi.org/10.1016/j.agrformet.2013.04.004

Immerzeel, W., Petersen, L., Ragettli, S., & Pellicciotti, F. (2014). The importance of observed gradients of air temperature and precipitation for modeling runoff from a glacierized watershed in the Nepalese Himalayas. *Water Resources Research*, *50*, 2212–2226. https://doi.org/10.1002/2013WR014506

Jarvis, C. H., & Stuart, N. (2001). A comparison among strategies for interpolating maximum and minimum daily air temperatures. Part II: The interaction between number of guiding variables and the type of interpolation method. *Journal of Applied Meteorology*, *40*(6), 1075–1084. https://doi.org/10.1175/1520-0450(2001)040%3C1075:ACASFI%3E2.0.CO;2

Kang, S., Xu, Y., You, Q., Flügel, W.-A., Pepin, N., & Yao, T. (2010). Review of climate and cryospheric change in the Tibetan Plateau. *Environmental Research Letters*, *5*(1), 015101. https://doi.org/10.1088/1748-9326/5/1/015101

Kattel, D. B., Yao, T., & Panday, P. K. (2017). Near-surface air temperature lapse rate in a humid mountainous terrain on the southern slopes of the eastern Himalayas. *Theoretical and Applied Climatology*, 1–13.

Kattel, D. B., Yao, T., Yang, K., Tian, L., Yang, G., & Joswiak, D. (2013). Temperature lapse rate in complex mountain terrain on the southern slope of the central Himalayas. *Theoretical and Applied Climatology*, *113*(3-4), 671–682. https://doi.org/10.1007/s00704-012-0816-6

Kattel, D. B., Yao, T., Yang, W., Gao, Y., & Tian, L. (2015). Comparison of temperature lapse rates from the northern to the southern slopes of the Himalayas. *International Journal of Climatology*, *35*(15), 4431–4443. https://doi.org/10.1002/joc.4297

Kilibarda, M., Hengl, T., Heuvelink, G. B. M., Gräler, B., Pebesma, E., Perčec Tadić, M., & Bajat, B. (2014). Spatio-temporal interpolation of daily temperatures for global land areas at 1 km resolution. *Journal of Geophysical Research: Atmospheres*, *119*, 2294–2313. https://doi.org/10.1002/2013JD020803

Kollas, C., Randin, C. F., Vitasse, Y., & Körner, C. (2014). How accurately can minimum temperatures at the cold limits of tree species be extrapolated from weather station data? *Agricultural and Forest Meteorology*, *184*, 257–266. https://doi.org/10.1016/j.agrformet.2013.10.001

Li, X., Wang, L., Chen, D., Yang, K., Xue, B., & Sun, L. (2013). Near-surface air temperature lapse rates in the mainland China during 1962–2011. *Journal of Geophysical Research: Atmospheres*, *118*, 7505–7515. https://doi.org/10.1002/jgrd.50553

Li, Y., Zeng, Z., Zhao, L., & Piao, S. (2015). Spatial patterns of climatological temperature lapse rate in mainland China: A multi–time scale investigation. *Journal of Geophysical Research: Atmospheres*, *120*, 2661–2675. https://doi.org/10.1002/2014JD022978

Li, Z.-L., Tang, B.-H., Wu, H., Ren, H., Yan, G., Wan, Z., et al. (2013). Satellite-derived land surface temperature: Current status and perspectives. *Remote Sensing of Environment*, *131*, 14–37. https://doi.org/10.1016/j.rse.2012.12.008

Lilleøren, K. S., Etzelmüller, B., Gärtner-Roer, I., Kääb, A., Westermann, S., & Guðmundsson, Á. (2013). The distribution, thermal characteristics and dynamics of permafrost in Tröllaskagi, northern Iceland, as inferred from the distribution of rock glaciers and ice-cored moraines. *Permafrost and Periglacial Processes*, *24*(4), 322–335. https://doi.org/10.1002/ppp.1792

Lin, X., Zhang, W., Huang, Y., Sun, W., Han, P., Yu, L., & Sun, F. (2016). Empirical estimation of near-surface air temperature in China from MODIS LST data by considering physiographic features. *Remote Sensing*, *8*(8), 629. https://doi.org/10.3390/rs8080629

Liu, C., Cao, G., Zhang, M., Niu, X., Xu, W., & Fan, J. (2013). Influence of temporal and spatial variability on estimation of air temperatures from MODIS land surface temperatures. *Remote Sensing Technology and Application*, *28*(5), 831–835.

Liu, W., Zhang, D., Liu, J., Shen, Y., Xiao, C., Liu, J., et al. (2013). A study on temperature lapse rate on the northern and southern slopes of the central Himalayas. *Journal of Arid Meteorology*, *31*(2), 240–245.

Liu, X., & Chen, B. (2000). Climatic warming in the Tibetan Plateau during recent decades. *International Journal of Climatology*, *20*(14), 1729–1742. https://doi.org/10.1002/1097-0088(20001130)20:14%3C1729::AID-JOC556%3E3.0.CO;2-Y

Luo, Y., Arnold, J., Liu, S. Y., Wang, X. Y., & Chen, X. (2013). Inclusion of glacier processes for distributed hydrological modeling at basin scale with application to a watershed in Tianshan Mountains, Northwest China. *Journal of Hydrology*, *477*, 72–85. https://doi.org/10.1016/j.jhydrol.2012.11.005

Ma, N., Niu, G. Y., Xia, Y., Cai, X., Zhang, Y., Ma, Y., & Fang, Y. (2017). A systematic evaluation of Noah-MP in simulating land-atmosphere energy, water, and carbon exchanges over the continental United States. *Journal of Geophysical Research: Atmospheres*, *122*, 12,245–12,268. https://doi.org/10.1002/2017JD027597

Ma, N., Zhang, Y., Szilagyi, J., Guo, Y., Zhai, J., & Gao, H. (2015). Evaluating the complementary relationship of evapotranspiration in the alpine steppe of the Tibetan Plateau. *Water Resources Research*, *51*, 1069–1083. https://doi.org/10.1002/2014WR015493

Marshall, S. J., Sharp, M. J., Burgess, D. O., & Anslow, F. S. (2007). Near-surface-temperature lapse rates on the Prince of Wales Icefield, Ellesmere Island, Canada: Implications for regional downscaling of temperature. *International Journal of Climatology*, *27*(3), 385–398. https://doi.org/10.1002/joc.1396

Meyer, H., Katurji, M., Appelhans, T., Müller, M., Nauss, T., Roudier, P., & Zawar-Reza, P. (2016). Mapping daily air temperature for Antarctica based on MODIS LST. *Remote Sensing*, *8*(9), 732. https://doi.org/10.3390/rs8090732

Minder, J. R., Mote, P. W., & Lundquist, J. D. (2010). Surface temperature lapse rates over complex terrain: Lessons from the Cascade Mountains. *Journal of Geophysical Research*, *115*, D14122. https://doi.org/10.1029/2009JD013493

Mutiibwa, D., Strachan, S., & Albright, T. (2015). Land surface temperature and surface air temperature in complex terrain. *IEEE Journal of Selected Topics in Applied Earth Observations and Remote Sensing*, *8*(10), 4762–4774. https://doi.org/10.1109/JSTARS.2015.2468594

Nilsson, A. G. (2009). Near-surface temperature lapse rates over Arctic glaciers and their implications for temperature downscaling. *Journal of Climate*, *22*(16), 4281–4298.

Oyler, J. W., Dobrowski, S. Z., Holden, Z. A., & Running, S. W. (2016). Remotely sensed land skin temperature as a spatial predictor of air temperature across the conterminous United States. *Journal of Applied Meteorology and Climatology*, *55*(7), 1441–1457. https://doi.org/10.1175/JAMC-D-15-0276.1

Park, S. (2011). Integration of satellite-measured LST data into cokriging for temperature estimation on tropical and temperate islands. *International Journal of Climatology*, *31*(11), 1653–1664. https://doi.org/10.1002/joc.2185

Peon, J., Recondo, C., & Calleja, J. F. (2014). Improvements in the estimation of daily minimum air temperature in peninsular Spain using MODIS land surface temperature. *International Journal of Remote Sensing*, *35*(13), 5148–5166. https://doi.org/10.1080/01431161.2014.935831

Pepin, N. (2001). Lapse rate changes in northern England. *Theoretical and Applied Climatology*, *68*(1), 1–16.

Pepin, N., Bradley, R., Diaz, H., Baraër, M., Caceres, E., Forsythe, N., et al. (2015). Elevation-dependent warming in mountain regions of the world. *Nature Climate Change*, *5*(5), 424–430.

Pepin, N. C., Maeda, E. E., & Williams, R. (2016). Use of remotely sensed land surface temperature as a proxy for air temperatures at high elevations: Findings from a 5000 m elevational transect across Kilimanjaro. *Journal of Geophysical Research: Atmospheres*, *121*, 9998–10,015. https://doi.org/10.1002/2016JD025497

Petersen, L., Pellicciotti, F., Juszak, I., Carenzo, M., & Brock, B. (2013). Suitability of a constant air temperature lapse rate over an alpine glacier: Testing the Greuell and Böhm model as an alternative. *Annals of Glaciology*, *54*(63), 120–130. https://doi.org/10.3189/2013AoG63A477

Qu, P., Shi, R., Liu, C., & Zhong, H. (2011). The evaluation of MODIS data and geographic data for estimating near surface air temperature. *Remote Sensing for Land & Resources*, *37*(4), 78–82.

Rolland, C. (2003). Spatial and seasonal variations of air temperature lapse rates in Alpine regions. *Journal of Climate*, *16*(7), 1032–1046. https://doi.org/10.1175/1520-0442(2003)016%3C1032:SASVOA%3E2.0.CO;2

Shamir, E., & Georgakakos, K. P. (2014). MODIS land surface temperature as an index of surface air temperature for operational snowpack estimation. *Remote Sensing of Environment*, *152*, 83–98. https://doi.org/10.1016/j.rse.2014.06.001

Stahl, K., Moore, R. D., Floyer, J. A., Asplin, M. G., & McKendry, I. G. (2006). Comparison of approaches for spatial interpolation of daily air temperature in a large region with complex topography and highly variable station density. *Agricultural and Forest Meteorology*, *139*(3–4), 224–236. https://doi.org/10.1016/j.agrformet.2006.07.004

Sun, R., Zhang, X. Q., Sun, Y., Zheng, D., & Fraedrich, K. (2013). SWAT-based streamflow estimation and its responses to climate change in the Kadongjia River watershed, southern Tibet. *Journal of Hydrometeorology*, *14*(5), 1571–1586. https://doi.org/10.1175/jhm-d-12-0159.1

Tang, Z. G., Wang, J., Li, H. Y., & Yan, L. L. (2013). Spatiotemporal changes of snow cover over the Tibetan plateau based on cloud-removed moderate resolution imaging spectroradiometer fractional snow cover product from 2001 to 2011. *Journal of Applied Remote Sensing*, *7*, 14.

Tonini, F., Dillon, W. W., Money, E. S., & Meentemeyer, R. K. (2016). Spatio-temporal reconstruction of missing forest microclimate measurements. *Agricultural and Forest Meteorology*, *218*, 1–10. https://doi.org/10.1016/j.agrformet.2015.11.004

Walther, G.-R., Post, E., Convey, P., Menzel, A., Parmesan, C., Beebee, T. J., et al. (2002). Ecological responses to recent climate change. *Nature*, *416*(6879), 389–395. https://doi.org/10.1038/416389a

Wan, Z. (2014). New refinements and validation of the collection-6 MODIS land-surface temperature/emissivity product. *Remote Sensing of Environment*, *140*, 36–45. https://doi.org/10.1016/j.rse.2013.08.027

Wang, L., Sun, L., Shrestha, M., Li, X., Liu, W., Zhou, J., et al. (2016). Improving snow process modeling with satellite-based estimation of near-surface-air-temperature lapse rate. *Journal of Geophysical Research: Atmospheres*, *121*, 12,005–12,030. https://doi.org/10.1002/2016JD025506

Wang, W., Liang, S., & Meyers, T. (2008). Validating MODIS land surface temperature products using long-term nighttime ground measurements. *Remote Sensing of Environment*, *112*(3), 623–635. https://doi.org/10.1016/j.rse.2007.05.024

Wolfe, R. E., Nishihama, M., Fleig, A. J., Kuyper, J. A., Roy, D. P., Storey, J. C., & Patt, F. S. (2002). Achieving sub-pixel geolocation accuracy in support of MODIS land science. *Remote Sensing of Environment*, *83*(1-2), 31–49. https://doi.org/10.1016/S0034-4257(02)00085-8

Wu, S. H., Jansson, P.-E., & Kolari, P. (2012). The role of air and soil temperature in the seasonality of photosynthesis and transpiration in a boreal Scots pine ecosystem. *Agricultural and Forest Meteorology*, *156*, 85–103.

Xu, W., & Liu, X. (2007). Response of vegetation in the Qinghai-Tibet Plateau to global warming. *Chinese Geographical Science*, *17*(2), 151–159.

Xu, Y., Knudby, A., & Ho, H. C. (2014). Estimating daily maximum air temperature from MODIS in British Columbia, Canada. *International Journal of Remote Sensing*, *35*(24), 8108–8121. https://doi.org/10.1080/01431161.2014.978957

Xu, Y. M., Qin, Z. H., & Shen, Y. (2012). Study on the estimation of near-surface air temperature from MODIS data by statistical methods. *International Journal of Remote Sensing*, *33*(24), 7629–7643. https://doi.org/10.1080/01431161.2012.701351

Yang, X., Zhang, T., Qin, D., Kang, S., & Qin, X. (2011). Characteristics and changes in air temperature and Glacier's response on the north slope of Mt. Qomolangma (Mt. Everest). *Arctic, Antarctic, and Alpine Research*, *43*(1), 147–160. https://doi.org/10.1657/1938-4246-43.1.147

Yao, T., Thompson, L. G., Mosbrugger, V., Zhang, F., Ma, Y., Luo, T., et al. (2012). Third pole environment (TPE). *Environmental Development*, *3*, 52–64. https://doi.org/10.1016/j.envdev.2012.04.002

Yao, Y. H., & Zhang, B. P. (2013). MODIS-based estimation of air temperature of the Tibetan Plateau. *Journal of Geographical Sciences*, *23*(4), 627–640. https://doi.org/10.1007/s11442-013-1033-7

Yu, J., Zhang, G., Yao, T., Xie, H., Zhang, H., Ke, C., & Yao, R. (2016). Developing daily cloud-free snow composite products from MODIS Terra-Aqua and IMS for the Tibetan Plateau. *IEEE Transactions on Geoscience and Remote Sensing*, *54*(4), 2171–2180. https://doi.org/10.1109/TGRS.2015.2496950

Zhang, F., Zhang, H., Hagen, S. C., Ye, M., Wang, D., Gui, D., et al. (2015). Snow cover and runoff modelling in a high mountain catchment with scarce data: Effects of temperature and precipitation parameters. *Hydrological Processes*, *29*(1), 52–65. https://doi.org/10.1002/hyp.10125

Zhang, G., Yao, T., Xie, H., Kang, S., & Lei, Y. (2013). Increased mass over the Tibetan Plateau: From lakes or glaciers? *Geophysical Research Letters*, *40*, 2125–2130. https://doi.org/10.1002/grl.50462

Zhang, H., Zhang, F., Ye, M., Che, T., & Zhang, G. (2016). Estimating daily air temperatures over the Tibetan Plateau by dynamically integrating MODIS LST data. *Journal of Geophysical Research: Atmospheres*, *121*, 11,425–11,441. https://doi.org/10.1002/2016JD025154

Zhang, H., Zhang, F., Zhang, G., He, X., & Tian, L. (2016). Evaluation of cloud effects on air temperature estimation using MODIS LST based on ground measurements over the Tibetan Plateau. *Atmospheric Chemistry and Physics*, *16*(21), 13,681–13,696. https://doi.org/10.5194/acp-16-13681-2016

Zhang, H., Zhang, F. A. N., Zhang, G., Ma, Y., Yang, K. U. N., & Ye, M. (2018). Daily air temperature estimation on glacier surfaces in the Tibetan Plateau using MODIS LST data. *Journal of Glaciology*, *64*(243), 132–147. https://doi.org/10.1017/jog.2018.6

Zhang, L., Su, F., Yang, D., Hao, Z., & Tong, K. (2013). Discharge regime and simulation for the upstream of major rivers over Tibetan Plateau. *Journal of Geophysical Research: Atmospheres*, *118*, 8500–8518. https://doi.org/10.1002/jgrd.50665

Zhang, W., Huang, Y., Yu, Y. Q., & Sun, W. J. (2011). Empirical models for estimating daily maximum, minimum and mean air temperatures with MODIS land surface temperatures. *International Journal of Remote Sensing*, *32*(24), 9415–9440. https://doi.org/10.1080/01431161.2011.560622

Zhao, D., Zhang, W., & Xu, S. (2007). A neural network algorithm to retrieve nearsurface air temperature from landsat ETM+ imagery over the Hanjiang river basin, China, paper presented at geoscience and remote sensing symposium, 2007. IGARSS 2007. IEEE international, Barcelona, 23–28 July 2007.

Zhou, W., Peng, B., Shi, J., Wang, T., Dhital, Y. P., Yao, R., et al. (2017). Estimating high resolution daily air temperature based on remote sensing products and climate reanalysis datasets over glacierized basins: A case study in the Langtang valley, Nepal. *Remote Sensing*, *9*(9), 959. https://doi.org/10.3390/rs9090959

Zhu, W., Lű, A., & Jia, S. (2013). Estimation of daily maximum and minimum air temperature using MODIS land surface temperature products. *Remote Sensing of Environment*, *130*(0), 62–73. https://doi.org/10.1016/j.rse.2012.10.034